



Real-time assessment of potential seismic migration within a monitoring network using Red-flag SARA

Chiou Ting Tan^{a,*}, Benoît Taisne^{a,b}, Jurgen Neuberg^c, Ahmad Basuki^d

^a Earth Observatory of Singapore, Nanyang Technological University, 50 Nanyang Avenue, N2-01b-30, Singapore 639798, Singapore

^b Asian School of the Environment, Nanyang Technological University, 50 Nanyang Avenue, N2-01b-24, Singapore 639798, Singapore

^c Institute of Geophysics and Tectonics, School of Earth and Environment, The University of Leeds, Leeds LS2 9JT, United Kingdom

^d Center for Volcanology and Geological Hazard Mitigation, Jl. Diponegoro 57, Bandung 40122, Indonesia

ARTICLE INFO

Article history:

Received 11 March 2019

Received in revised form 25 June 2019

Accepted 5 July 2019

Available online 07 July 2019

ABSTRACT

Magma opening new fluid pathways through the crust can generate migrating seismic sources following the trail of the magma. By using Seismic Amplitude Ratio Analysis (SARA), it is possible to detect this seismic migration simply from the amplitudes of continuous data recorded at different stations in a network, without having to do any picking of seismic phases. In this study, we present a modified method – Red-flag SARA, which adapts SARA for real-time monitoring. Red-flag SARA provides a quantitative tool to analyse amplitude ratios between stations in a network and detect temporal changes in these ratios. Since such changes imply seismic source location variations, Red-flag SARA is a handy tool during seismic crises to quickly answer the question of whether seismic activity, and therefore magma, is migrating or not. We tested Red-flag SARA on synthetic data and validated it using real data from two volcanoes – Piton de la Fournaise, Reunion Island, and Gede, Indonesia, for three scenarios: 1) magma migration ending as intrusion, 2) migration leading to eruption and 3) a burst of seismicity with no magma migration.

© 2019 The Authors. Published by Elsevier B.V. This is an open access article under the CC BY-NC-ND license (<http://creativecommons.org/licenses/by-nc-nd/4.0/>).

1. Introduction

One of the primary aims of volcano observatories is to monitor volcanoes and provide timely warnings of impending eruptions. Having more specific tools to analyse monitoring data would improve the forecasting capability of observatories. Typically at observatories, seismic monitoring is focussed on conventional techniques such as tabulating event counts, calculating RSAM, and when time permits, locating hypocentres of events. Less emphasized is the tracking of seismicity migration, particularly in real-time. Volcanic eruptions are often heralded by magma movement, which induces stress perturbations that are revealed by seismic swarms consisting of larger, discrete brittle-failure events, as well as less detectable smaller signals still contributing seismic energy. Any seismic migration indicates potential magma motion, and detecting such motion as early as possible is crucial for observatories. While seismic migration can also be inferred from computing hypocentre locations based on phase picking, during swarms of huge numbers of events, with events sometimes merging, this is not practical and, if feasible at all, requires post-processing for more precise results.

Here we address this shortcoming by improving upon the Seismic Amplitude Ratio Analysis (SARA) method (Taisne et al., 2011), making the analysis more quantitative and robust so that automated real-time monitoring can easily be employed at observatories.

SARA was implemented to simply detect seismicity migration by tracking the temporal evolution of seismic amplitude ratios from different seismic stations in a network, i.e. $\text{Amplitude}_{\text{station}_i} / \text{Amplitude}_{\text{station}_j}$. In contrast, previous studies by Battaglia and Aki (2003) and Jolly et al. (2002) made use of the varying seismic amplitudes recorded at different stations in a network together with the attenuation law to map out source locations. However, these methods require good knowledge of the site amplification factor and instrument response of each station, which might not be readily available. If only a simple yes/no answer to migration is required, the need for all this information is eliminated. Hence, the main objective of this study is to provide an automated process to alert observers to changes in seismic source location, not the actual location itself. We name this tool Red-flag SARA, as migrating seismicity will take the shape of a red-flag in our final step of the analysis. Of course, if the seismic traces are corrected for instrument response and site amplification, event locations can be deduced (Caudron et al., 2015; Taisne et al., 2011), and seismic sources can be tracked from the starting point all the way to the eruptive vent (or intrusion point), as demonstrated by Caudron et al. (2018) at

* Corresponding author.

E-mail addresses: chiouting@ntu.edu.sg (C.T. Tan), BTaisne@ntu.edu.sg (B. Taisne), J.Neuberg@leeds.ac.uk (J. Neuberg), ahmad.basuki@esdm.go.id (A. Basuki).

Bárðarbunga. We tested Red-flag SARA by applying it to synthetic seismograms simulating seismic migration, and validated it using real seismic data which was associated to known magma migration.

2. Data sources

2.1. Synthetics

We used synthetic seismograms simulating migrating events to test our methodology. Each event is separated by 2 s, at the source location, and the source-receiver travel time is computed using shear-wave velocity in order to get a new time series representing arrival times of waves reaching a given station. The seismogram at a given station was then generated by convolving a 10 Hz, 5 s long Morlet wavelet with the associated time series of spikes. The 2 s interval ensure that the events are overlapping in the seismogram. Amplitudes of events were calculated using the following equation (Battaglia and Aki, 2003):

$$A(r) = A_0 \frac{e^{-Br}}{r^n},$$

with,

$$B = \frac{\pi f}{Q\beta},$$

where A_0 is the amplitude at the source, $n = 1$ for body waves and $n = 0.5$ for surface waves, f is mean frequency, β is seismic shear-wave velocity and Q is the quality factor for attenuation, and r is the distance between source and station. Since we are interested only in the temporal changes in the amplitude ratios, the exact values used for the various parameters are not relevant for our analysis. Constant crustal properties and a constant n are assumed. Even though it is possible for earthquakes to become dominated by surface waves rather than body waves as they approach the surface in a vertical migration and become shallow enough, this is not an issue since in both cases, migration will still effect a temporal change in the amplitude ratios.

The actual seismic network geometry at Gede Volcano, Indonesia (Fig. 1) was used for the migration simulation. After defining the start and end locations as well as the migration speed, regularly-spaced migration points from the start to the end locations were determined based on migration speed and a 2-second event interval (Fig. 2(a)).

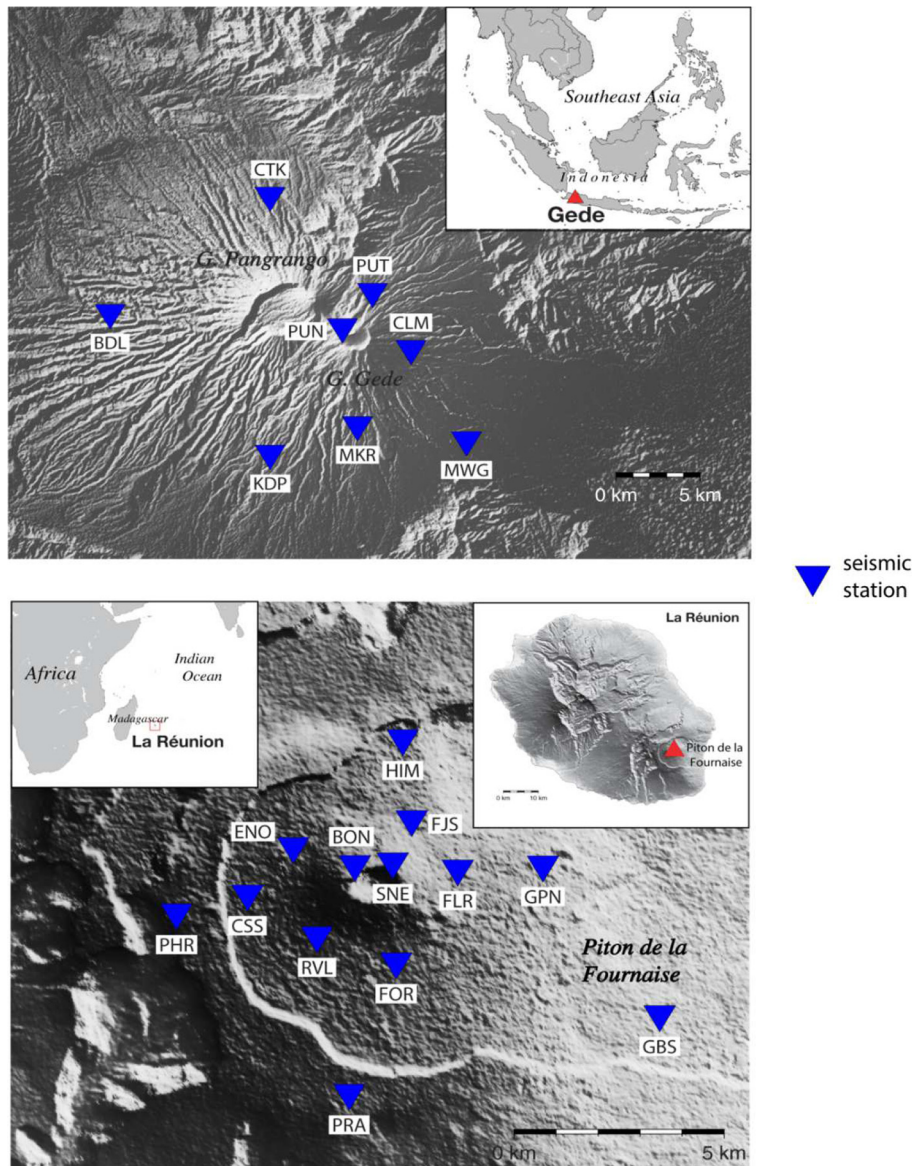


Fig. 1. Top: Seismic network and location map (inset) of Gede Volcano (Top) and Piton de la Fournaise (Bottom).

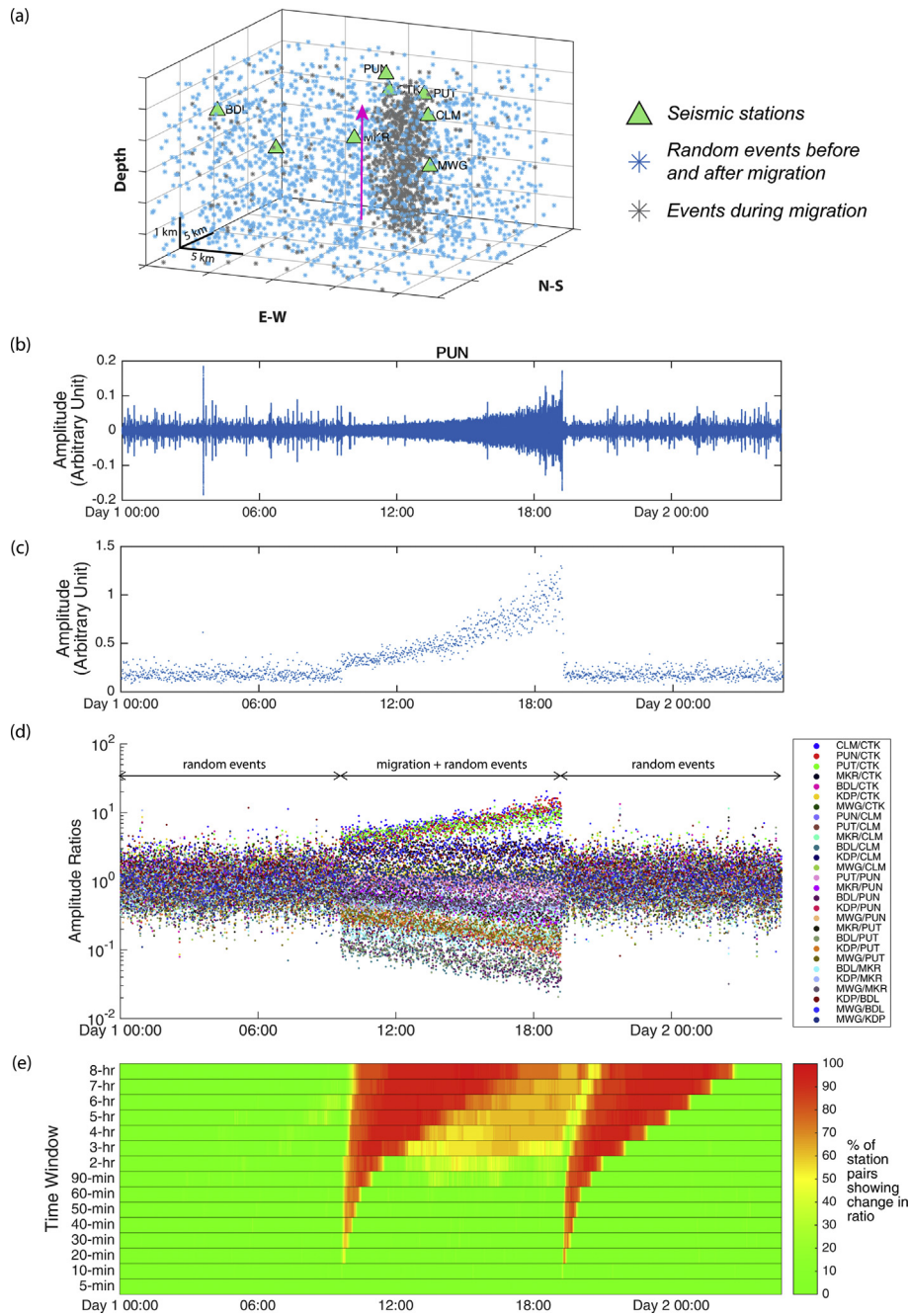


Fig. 2. Results for simulated vertical migration from 2 km below sea level to 2 km above sea level. (a). 3-D plot showing seismic network and event locations. (b). Raw synthetic seismogram for station PUN. (c). Enveloped, decimated, processed 1-minute data for station PUN. (d). Time series of amplitude ratios for all possible station pairs. (e). Time series showing the percentage of station pairs exhibiting changes in amplitude ratios. Red colours indicate greater confidence that migration is happening. Calculation was done with moving windows, shifting by 1 min from one window to the next. Every point plotted in time reflects the ratio changes in the time window just before the point. We assumed similar random events before the start of the plot in order to have data for the beginning of the time series before a complete time window. The smallest time window which shows clear detection of amplitude ratio changes gives an estimation of when migration ends. With larger time windows like 7-h or 8-h windows, the end of the migration seems to be later than it actually is because at this later time, the larger windows still capture the earlier amplitude ratio changes. (For interpretation of the references to colour in this figure legend, the reader is referred to the web version of this article.)

Migrating event locations were generated following Gaussian distributions around the migration points with pre-defined standard deviations. This was done instead of directly using the migration points as event locations in order to introduce some uncertainty, and hence mimicking natural system variability (see Section 5.3). We refer to the volume containing events within one standard deviation as ‘source volume’.

The final synthetic seismogram was completed by superimposing the migrating events to random events before, during and after the migration throughout the whole network to simulate background seismicity. Although such background seismicity might not be very realistic, it

serves to create a high level of uncertainty in the amplitude ratios and thus demonstrate that the method will work even under such circumstances. However, more realistic examples of background seismicity like a distal VT swarm (White and McCausland, 2016) or seismicity along a local fault, were also considered to illustrate the type of amplitude ratio patterns that might be expected from these common situations. Since these situations do not involve any migration, they are not expected to affect the amplitude ratio patterns. The results for these examples are described in Appendix A. During the migration, the rate of occurrence of migration events was set to be four times the rate of

background events. It is not necessary for the migration event rate to be higher than the background event rate in order for a trend in amplitude ratios to be detected (see Appendix C). All events (both migration and random) had source amplitudes which varied randomly over two orders of magnitude.

2.2. Real data

Seismic data from two volcanoes, Gede (West Java, Indonesia) and Piton de la Fournaise (La Réunion) were used to validate our methodology (Fig. 1). At both volcanoes, data from a mix of short period and broadband instruments with sampling frequencies of either 50 Hz or 100 Hz were used. No site amplification or instrument response was corrected for. At Gede, seismic swarms often occur with no associated eruptive activity. We selected a swarm in July 2015 with >120 volcano-tectonic (VT) events to which we apply our method. For Piton de la Fournaise, an intrusive event in May 2017 and an extrusion event in July 2015, both with associated seismic activity, were used.

3. Method

The basic concept behind tracking seismic amplitude ratios between different stations in a network over time has been described in Taisne et al. (2011). Considering that independent pairs of stations are used and that attenuation is likely to stay relatively stable over the timescale of short swarm periods, any change in the amplitude ratios will have to be attributed to a change in the seismic source location, which therefore points to stress migration and, potentially, fluid migration. Since we are interested in the higher frequency regime, we can assume an isotropic radiative pattern (Morioka et al., 2017).

3.1. Data processing to obtain amplitude ratios

Raw data have been first filtered between 5 and 15 Hz. The Hilbert transform has been applied and the absolute value obtained to get the amplitude envelope of the signal. The resulting data are decimated by taking the median for every second in order to remove transient spikes arising from telemetry, electronic or instrument noise and/or the way gaps are filled by data acquisition systems. Further processing has been applied by summing the data over a given time window which needs to be longer than the largest differential traveltime across the network, defined by the furthest distance between two stations and the assumed s-wave velocity. This is to ensure that the seismic energy calculated at every station for each moment in time is from the same source. Consideration of data size, computational time and ease of computation and result interpretation in later steps should also be factored into the decision on the time window size to sum over. In our study, the amplitude ratios for all possible station pairs are computed using summation over a 1-minute window, corresponding to a differential traveltime across a network well beyond the size of most networks.

3.2. Using correlation to quantitatively determine temporal amplitude ratio changes

In previous studies employing SARA, the amplitude ratios were plotted and any changes through time were identified simply by eye. This is sufficient if the ratio changes are large and obvious. However, for small changes and low signal to noise ratios, the results could be subjective and inconsistent. Here we suggest a quantitative approach to detect changes in the amplitude ratio using the Mann-Kendall trend test (Kendall and Gibbons, 1990), which identifies monotonic trends in data.

The general idea is that if the amplitude ratios increase or decrease with time, they would be more highly correlated with time than if the ratios are staying constant. The Mann-Kendall trend test involves computation of Kendall's correlation coefficient, τ , and the statistical parameter p -value. In our case, we set a null hypothesis that there is no trend

in the amplitude ratios, and a significance level of 0.01, i.e., if the calculated p -value is <0.01, we are >99% confident that the observed trend is not due to randomness and thus we reject the null hypothesis and conclude that there is a trend in the amplitude ratios. Due to the way τ is calculated, a step function can also result in a p -value that is smaller than 0.01, giving rise to a trend detection. This is demonstrated in Appendix B, and explains why in some of the examples presented later, a strong trend detection occurs at the start and end of a migration episode.

For each pair of stations, the trend test is applied through a moving time window across the whole time series of amplitude ratios, and a simple 0 (p -value > 0.01, no trend) or 1 (p -value < 0.01, trend exists) is assigned to each time window. Because the length of the time window used in determining a potential trend greatly influences the results, and the dynamics of the migration can vary, we conduct the trend test for a variety of window sizes. The process is repeated for all possible station pairs and the total number of station pairs which exhibit a trend in each time window is recorded. A final figure is then generated to display the percentage of station pairs which show changes in amplitude ratios through time for all time window sizes (Fig. 2). Note that at each point in time, the result/colour plotted is for the analysis of the data in the latest time window up to that point in time. The range of window sizes used should include windows sufficiently small to facilitate estimation of when migration ends (see Fig. 2), and windows sufficiently large to capture slow and noisy migration where trends become apparent only after a relatively long time.

3.3. Background noise removal

At some locations, it is inevitable to record the background noise contributed by diurnal and (to a smaller extent) seasonal cycles (Fig. 3). Therefore, changes in the computed amplitude ratios implying seismic migration could be masked by background noise cycles which cause amplitude ratios to change as well (see Section 5.5). The following steps were taken to estimate the diurnal background noise:

1. Select a period of quiet time, at least one week.
2. Sort the 1-minute data into 24 hourly bins, for the entire time period.
3. Compute for each hourly bin the median and median absolute deviation.
4. Plot medians for each bin to obtain the hourly background noise profile over the course of all days considered (Fig. 3).

To isolate the relevant seismic activity from the diurnal background noise, we considered each hour of the day and kept only data three median absolute deviations above the estimated background noise.

As data not significantly higher than background noise are discarded, data gaps are created which will affect the percentage of station pairs showing changes in amplitude ratio – a low percentage does not always reflect that most station pairs have constant amplitude ratios, but might instead be due to the fact that station pairs have these data gaps. In light of this, when background noise removal is involved, it should be noted that the percentage of station pairs displaying changes in amplitude ratio is actually the percentage of station pairs having detectable seismic energy and showing changes in amplitude ratio.

3.4. Testing on synthetics

We applied our method to synthetic seismograms simulating both horizontal and vertical migration. The synthetic seismograms were put through the methods described in Sections 3.1 and 3.2, except filtering, since they were generated at 10 Hz, hence in the 5–15 Hz range. Background noise removal was also unnecessary because there was no diurnal or seasonal variation introduced in the synthetic seismograms.

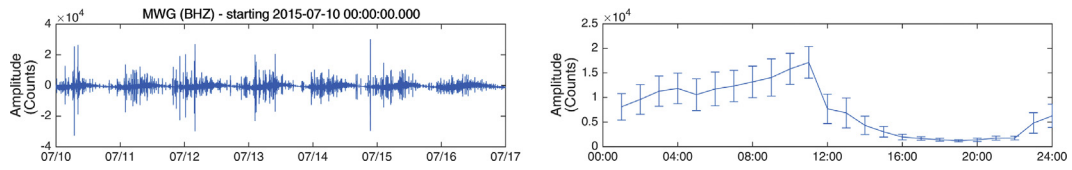


Fig. 3. Left: Seismogram at station MWG, where diurnal cycle is obvious. Right: Hourly background noise profile for station MWG computed using 1 week of data, with median absolute deviation shown.

For horizontal migration, events were set to migrate 10 km from west to east across the part of the network closest to the summit, and at a depth of 1 km below sea level. For vertical migration, events were set to migrate from 2 km below sea level to 2 km above sea level (but

not reaching the surface), and also from 2 km below sea level all the way up to the surface. In all cases, migration speed was set at 10 km per day, typical for magma movement (see Section 5.3 for discussion). Fig. 4 shows the results for a simple episode of background seismicity

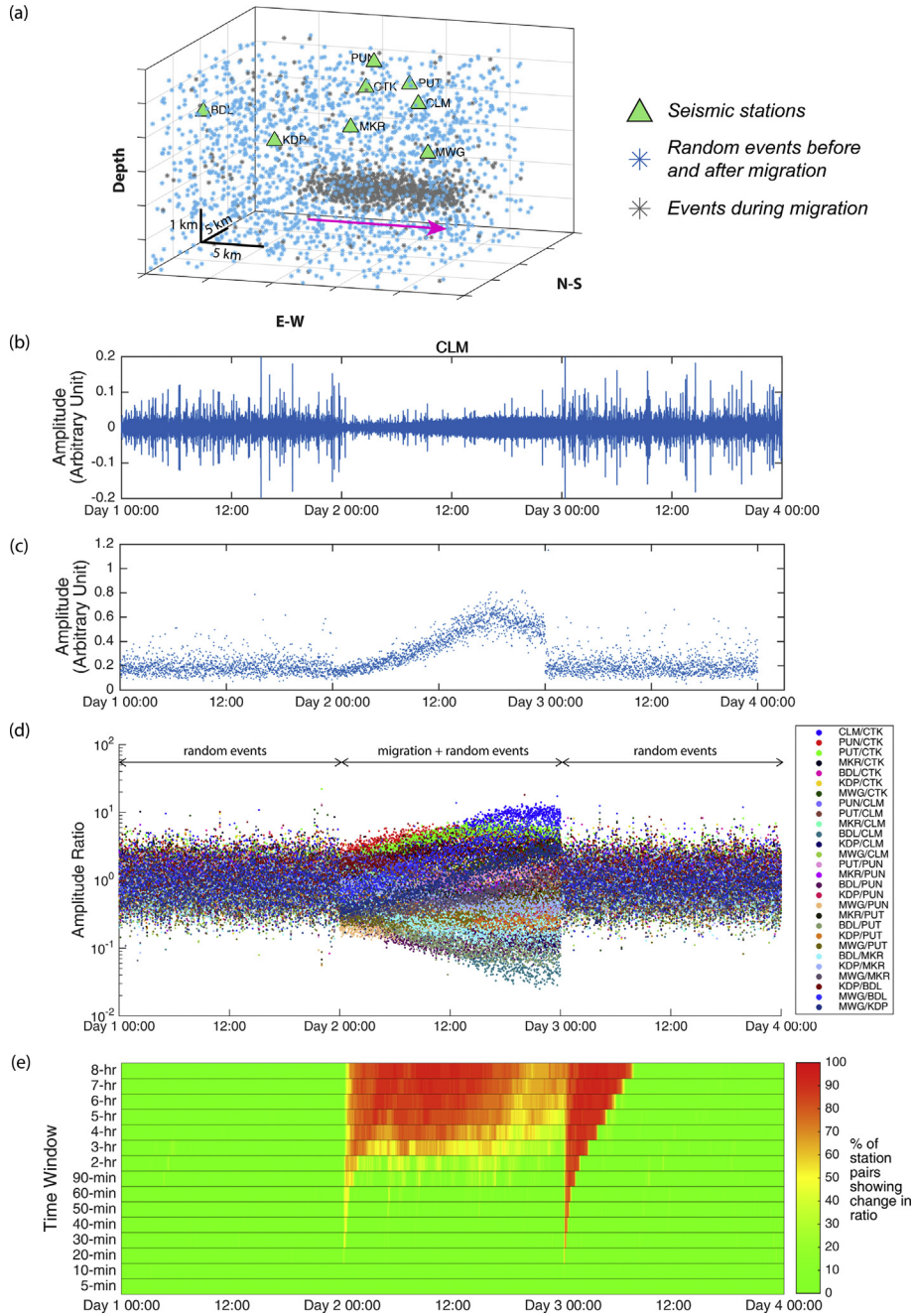


Fig. 4. Results for simulated horizontal migration from west to east at a depth of 1 km below sea level. Panels as for Fig. 2. A distinct change (green to red) can be clearly identified at the start of detectable migration where the percentage of station pairs showing a change in amplitude ratios undergoes a significant increase. During the migration, the percentage remains high (red). At the end of the eruption, the ratios show a rapid change back to the background values and this change shows up clearly in a similar fashion to the start of the migration. (For interpretation of the references to colour in this figure legend, the reader is referred to the web version of this article.)

shifting to horizontal migration from west to east and then back to background seismicity. A higher percentage of station pairs showing a change in amplitude ratios signifies greater confidence that migration is happening within the network at a location near to most stations. A distinct change (green to red) can be clearly identified at the start of detectable migration where the percentage of station pairs showing a change in amplitude ratios undergoes a significant increase. During the migration, the percentage remains high (red). At the end of the migration, the ratios show a rapid change back to the background values. As this change in amplitude ratios affects all station pairs detecting the migration, the result is that the termination of the migration is marked

by a high percentage of station pairs showing a change in amplitude ratios, in a similar fashion to the start of the migration. The results for this horizontal migration are similar to the results for vertical migration presented in Fig. 2.

Fig. 5 shows the results for a more complex episode where the background seismicity shifts towards migration, then to eruption tremor at the surface (simulated by localised merged events in a small source volume) and back to background seismicity when the eruption ends. As with the simple horizontal and vertical migration examples, the start of the migration and the end of the eruption are distinctly marked, and the migration can be clearly identified. However, the percentage

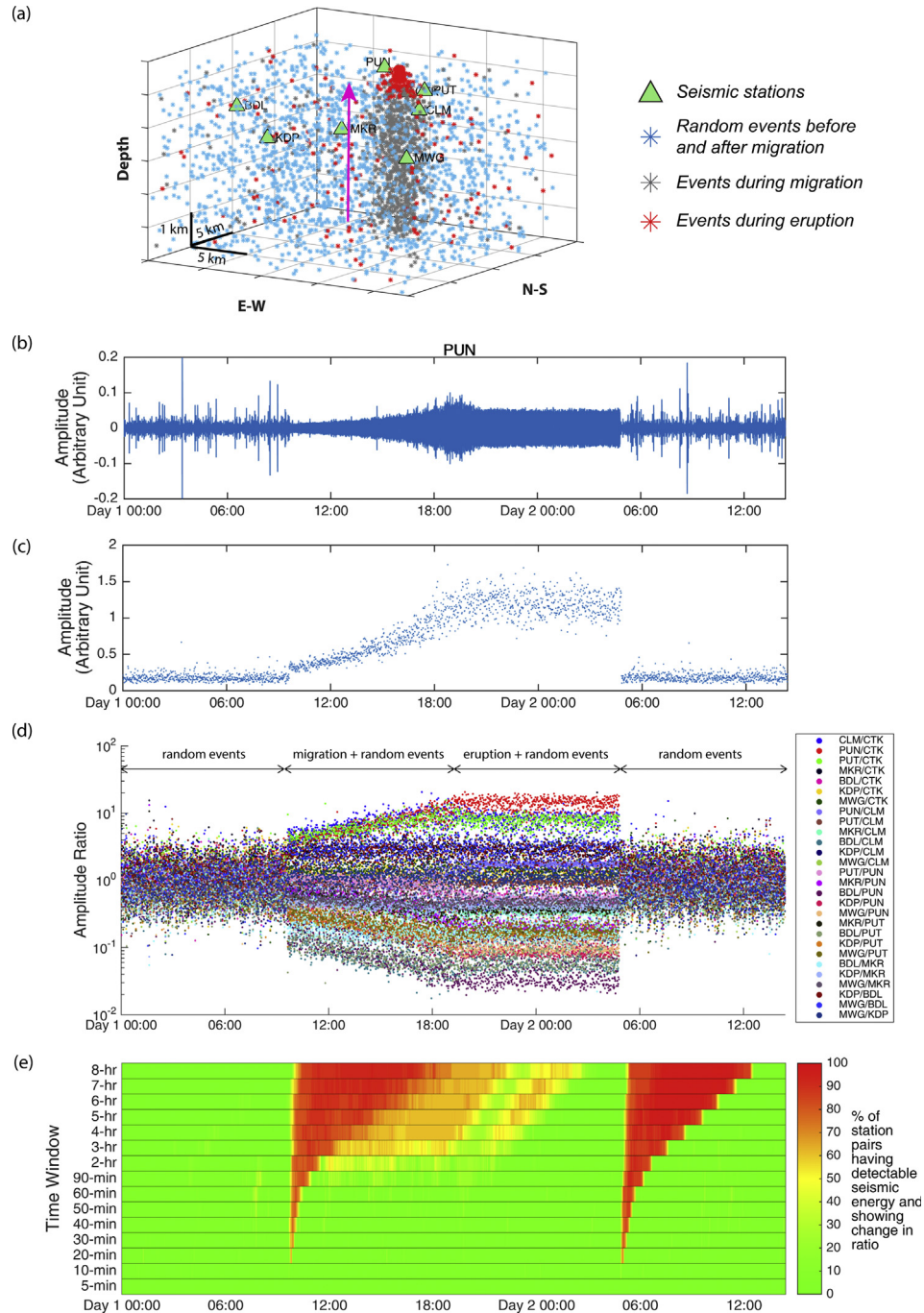


Fig. 5. Results for simulated vertical migration from 2 km below sea level to the surface, followed by an eruption. Panels as for Fig. 2. A distinct change (green to red) can be clearly identified at the start of detectable migration and at the end of the eruption. Eruption tremor appears as green because the seismic source location does not vary significantly. (For interpretation of the references to colour in this figure legend, the reader is referred to the web version of this article.)

of station pairs showing a change in amplitude ratios drops back to almost zero (green) once the migration ends and eruption tremor begins. Because the tremor is assumed to be generated at the eruptive vent, which is essentially where the migration stopped, there is no further change in location and amplitude ratios remain roughly the same, thus the percentage of station pairs showing a change in amplitude ratios falls back to a low value.

In some situations, amplitude ratios can show a reversal in trends, and this would give rise to a period during the migration when the red is interrupted by a short duration of green before returning to red, as seen in Fig. 5(c) at ~20:00. A more detailed explanation is provided in Appendix D.

4. Results – application to real data

4.1. Piton de la Fournaise, July 2015

After 24 h of seismic unrest accompanied by changes in deformation and gas measurements, a fissure eruption producing lava fountains started on 31 July 2015, lasting for 2 days. 90 min of high seismicity and 80 min of major deformation were recorded just before the start of the eruption (OVPF, 2015). This event is captured as shown in Fig. 6, similar to the results using synthetic seismograms (c.f. Fig. 5). Due to the short duration of the migration and given the variability in the ratios, window sizes larger than the migration duration would be needed for some station pairs to detect the migration – these station pairs would have detected the migration only after the migration had ended and eruption had started. However, about 40–50% of the station pairs would still detect a change approximately 20 min before the eruption started using smaller time windows.

4.2. Piton de la Fournaise, May 2017

On 17 May 2017, a seismic crisis with accompanying deformation was detected. However, no surface activity was observed except the formation of two new zones of fumaroles, suggesting an intrusive event where fractures opened but no lava was erupted. Volcanic-tectonic earthquakes were located at two zones, one under the summit and the other to the north-east sector (OVPF, 2017a, 2017b). Fig. 7 shows the results for this event. The start and end of the migration during the tremor is clearly detected, although a reversal of the amplitude ratio trends at mid-migration causes some difficulty in identifying the short trends, hence resulting in a green segment despite the continuing migration. This reversal of the amplitude ratio trends is possibly due to vertical or horizontal migration passing by one or two stations (see Appendix D). In the few hours from the start of the seismic crisis, migration is unclear. Detected changes in the amplitude ratios are more likely to have been triggered by the step change than a trend. This step change could be due to seismicity focussing at one source region, such as the initial rupturing of the magma storage region, then returning to elevated background levels similar to that recorded on 16th May. More detailed analysis would be needed to verify this.

4.3. Gede, July 2015

Fig. 8 shows the results for the July 2015 seismic swarm at Gede. This swarm was one of the many occurring occasionally with no subsequent eruptive activity. Although there were nearly 130 VT events recorded over the course of almost 48 h (PVMBG, 2015a), there was no indication

at all of migrating seismic sources – amplitude ratios were not changing for the majority of the station pairs. This result is in line with hypocentre locations computed for the VT events (Dannie Hidayat, personal communication), which were found to be spread out and did not follow any migration pattern. A further analysis was performed employing only the summit stations, to look for potential, shallow, localised migration. The results show that only one station is affecting the ratios (see Fig. 8 and discussion Section 5.5). More examples of non-migrating seismicity at Gede are included in Appendix E.

5. Discussion

5.1. Burst of seismicity with no/very slow migration versus seismic crises with magma movement

The July 2015 swarm at Gede was a case of a burst of seismicity but no migration of seismic sources. In contrast, for the seismic crisis in July 2015 at Piton de la Fournaise migration is evident. Comparing the results from these two episodes demonstrates that our method is able to clearly distinguish between bursts of seismicity with and without associated migration. This distinction could be useful in helping to determine if a volcano with detected increased seismicity is heading towards eruption.

5.2. Intrusion versus extrusion

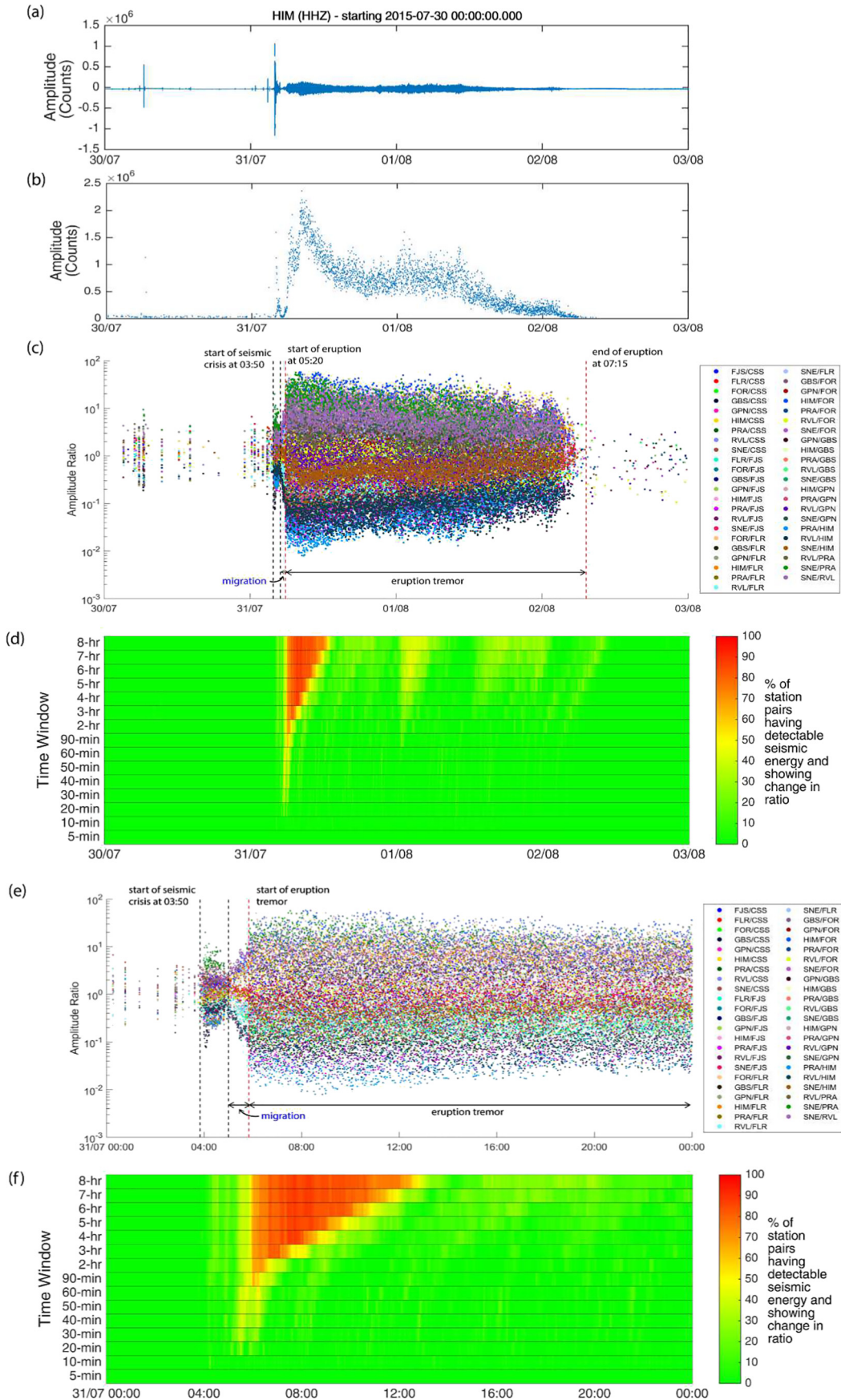
Besides detecting the onset and ending of a migration episode, our method also provides additional information on how the migration concluded – as an intrusion or an eruption. We used synthetic seismograms to provide proof of concept. If the migration ends in an eruption, the resulting pattern would be as described in Section 3.4 (Fig. 5). On the other hand, in the case of magma stalling at depth in an intrusive event, after the migration stops, seismicity returns to background activity, resulting in a rapid change in the amplitude ratios, as depicted by Figs. 2 and 4. In short, the difference in the patterns between an intrusive event and an extrusive one is that for an intrusion, there is a lack of the section corresponding to eruption tremor where the percentage of station pairs showing a change in amplitude ratios is low.

However, differentiation between an intrusion or eruption would not be possible if, 1) the eruption is a very short-lived one, too short to record the drop in percentage of station pairs showing a change in amplitude ratios before the percentage increases again at the end of the eruption; or 2) there is no continuing seismicity above background levels after the end of the eruption and hence no detection marking the end of the eruption, as was the case for Figs. 6 and 7.

5.3. Dynamics of seismic migration

During an episode of migration, seismic events will exhibit varying amplitudes and seismic sources are spread out in a certain volume around the migration front (Rubin, 1993) rather than moving sequentially forward with the migrating front. This variability in amplitude and location introduces a respective uncertainty in the amplitude ratios, hence, affecting how easily and reliably trends in the amplitude ratios are detected. This uncertainty is mapped into the percentage of station pairs exhibiting changes in amplitude ratios. A higher uncertainty makes it more difficult and requires larger time windows to detect trends. This is illustrated in Fig. 9, which depicts results from applying Red-flag SARA on synthetic data with varying source volumes

Fig. 6. Results for an eruption event at Piton de la Fournaise in July 2015. (a). Raw vertical-component seismogram for station HIM. (b). Filtered, enveloped, decimated 1-minute data for station HIM. (c). Time series of amplitude ratios for all possible station pairs. (d). Time series showing the percentage of station pairs with detectable seismic energy exhibiting changes in amplitude ratios. Calculation was done with moving windows, shifting by 1 min from one window to the next. Migration shows up clearly in red colours. The extension of the red area beyond the migration period is due to the larger window sizes used – the migration is still captured within the large window although the end of the window is past the migration period. (e) & (f). Zoom of Fig. 5(c) & (d). (For interpretation of the references to colour in this figure legend, the reader is referred to the web version of this article.)



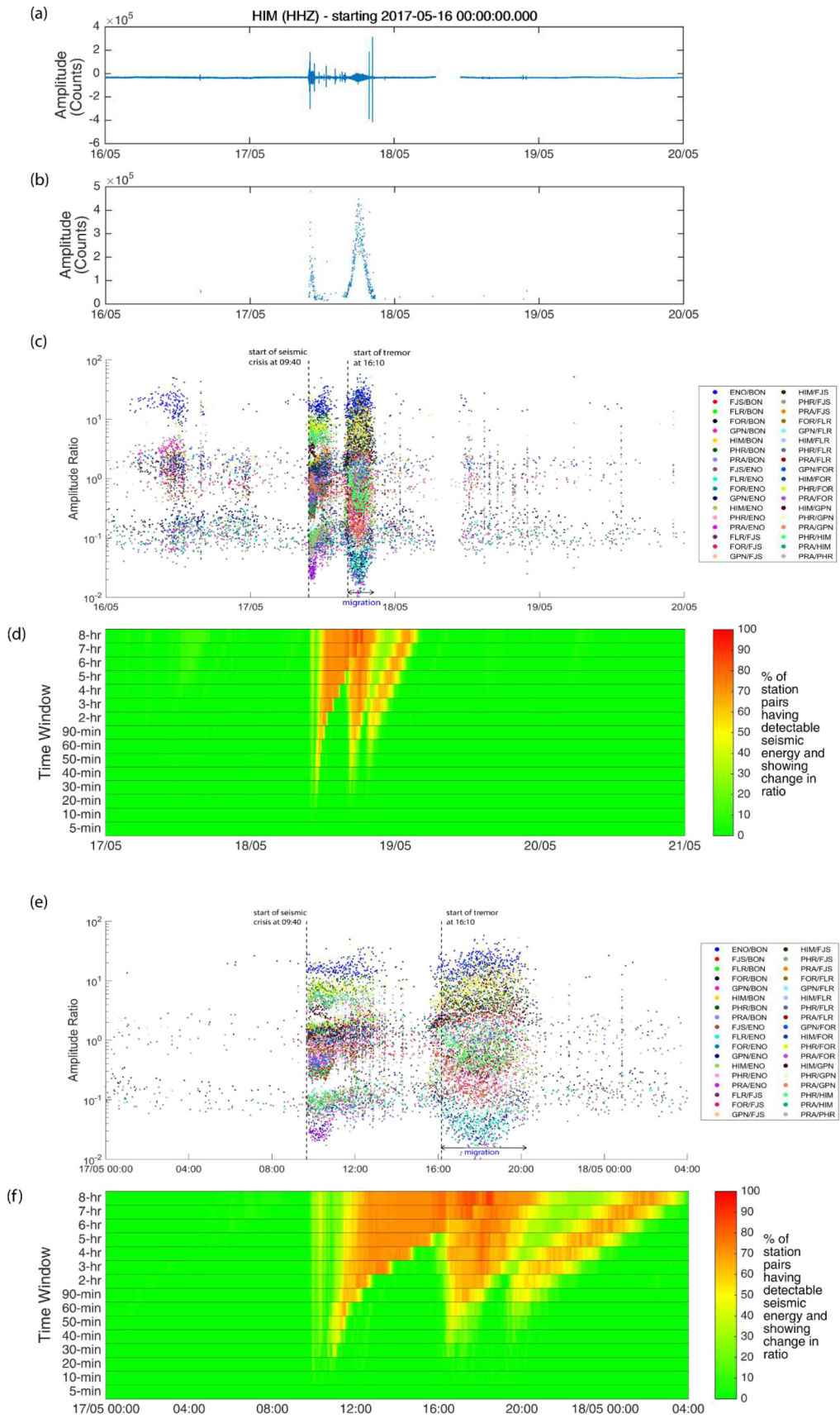


Fig. 7. Results for an intrusive event at Piton de la Fournaise in May 2017. Panels as for Fig. 6. Again, migration shows up in red colours. In the few hours from the start of the seismic crisis, migration is unclear. Detected changes in the amplitude ratios could be due to seismicity focussing at one source region, such as the initial rupturing of the magma storage region, then returning to elevated background levels. The green portion during the migration is due to the trends in amplitude ratios changing in opposite directions, hence appearing as ‘no trend’ if the time window is large enough to include the opposing trends. (For interpretation of the references to colour in this figure legend, the reader is referred to the web version of this article.)

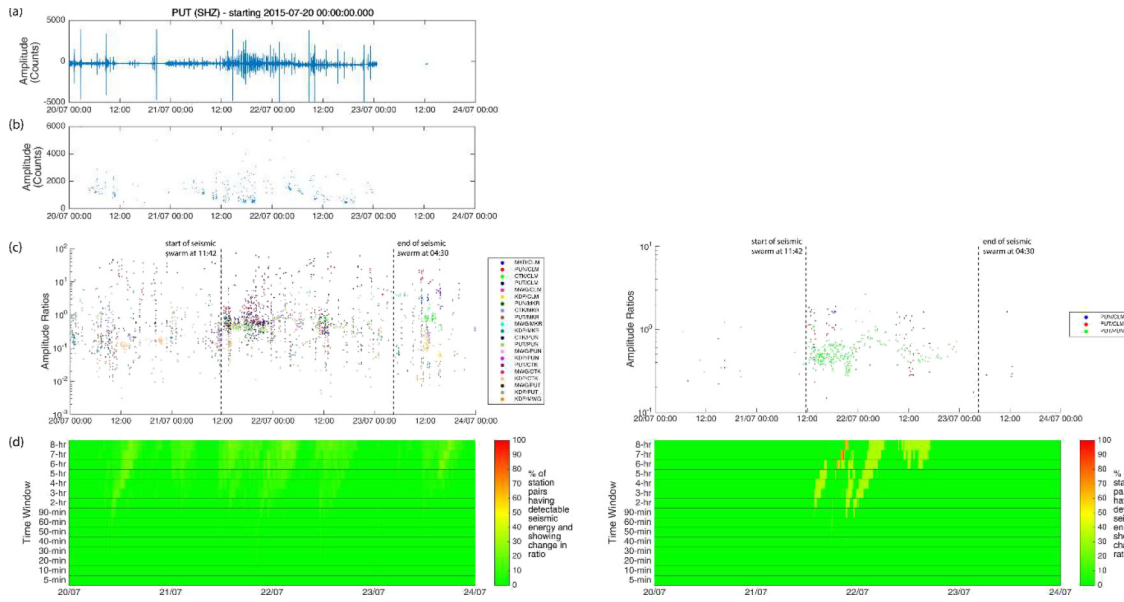


Fig. 8. Results for seismic swarm at Gede in July 2015. Left set of figures: Results using most of the network. Right: Results using only the summit stations. Most of the events were recorded only on these stations. (a). Raw vertical-component seismogram for station PUT. (b). Filtered, enveloped, decimated 1-minute data for station PUT. (c). Time series of amplitude ratios for all possible station pairs. (d). Time series showing the percentage of station pairs with detectable seismic energy exhibiting changes in amplitude ratios. Calculation was done with moving windows, shifting by 1 min from one window to the next. Note the effect of one station on a small network compared to a larger network.

(Table 1), and noting the minimum time window size required to detect the migration. Only one pair of stations (one near the summit [PUN] and the other on the flank [MWG]) was used, and migration was set to be vertical from deep (2 km below sea level) to near surface (2.5 km above sea level) not far from the summit station, at the same location as the example described in Section 3.4. The minimum detection time window size was determined by the proportion of time steps that detect a trend compared to a reference case with negligible source volume (Fig. 9). The size of the source volume, as defined in Section 2.1, can

be related to the state of stress of the volcano. A volcano which has not erupted in a long time would likely have a larger volume over which the sources are distributed in contrast to a recently active system that has established areas of stress release. If two similar consecutive intrusions occur at a particular volcano in a short time interval, the second intrusion will generate less seismic events due to stress being already released during the first one.

Another result of this variability in the amplitude ratio time series is its influence on the ease of detecting slow migration. Seismic migration

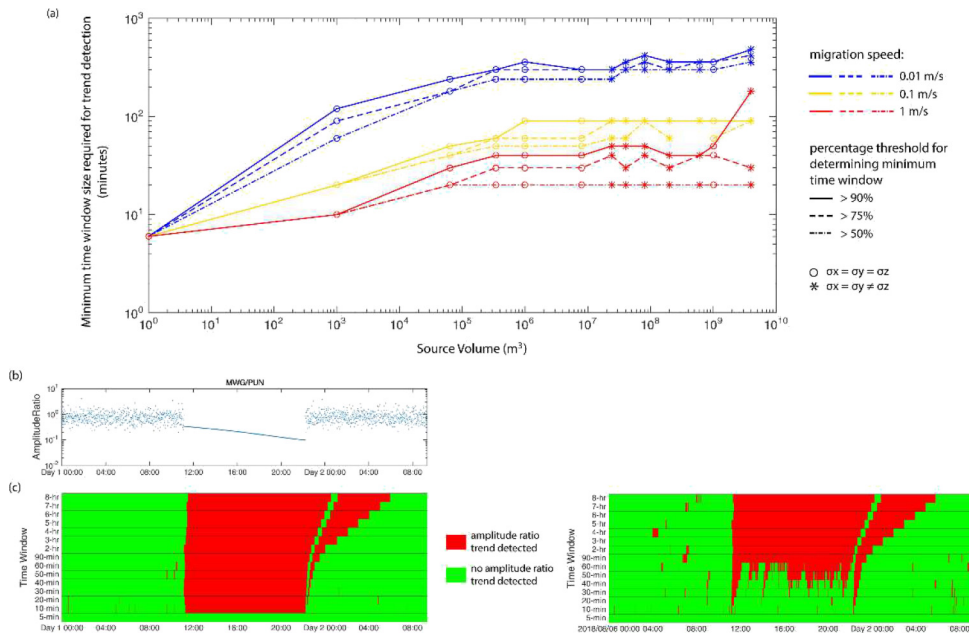


Fig. 9. (a). Plot showing the effects of migration speed and source volume size on the minimum time window size required to enable detection. The minimum source volume used is plotted at 1 m³ rather than 0 m³ to enable a logarithmic scale plot. Slower migration requires larger time windows for detection. Note that the plot was created based on one instance of generating event locations with Gaussian distributions. Repetition of the event location generation using the same parameters would not produce the exact same results. However, the important point of the plot is the trends observed, which remain similar with different iterations of event location generation. (b). Amplitude ratio for station pair MWG/PUN. (c). Left: Reference case with no spread of data. Right: Case with horizontal and vertical spreads of 100 m (standard deviation = 100 m). Percentage thresholds (90%, 75%, 50%) were used to objectively determine the minimum time window size. Towards the end of the migration, there is a short duration where detection of trend is lost. This is due to the way Kendall's correlation coefficient is calculated and is explained in Appendix B.

Table 1

Migrating event locations were generated following Gaussian distributions around the migration point with varying standard deviations ($\sigma_x, \sigma_y, \sigma_z$). Source volume is the volume containing the events within one standard deviation and represents the overall spread of the data.

Horizontal spread σ_x, σ_y (m)	0	5	20	35	50	100	100	100	100	500	500	500	1000
Vertical spread σ_z (m)	0	5	20	35	50	100	300	500	1000	100	300	500	500
Source volume (10^6 m^3)	0	0.001	0.064	0.343	1	8	24	40	80	200	600	1000	4000

could be the product of magma movement through dyke propagation, movement of hydrothermal fluids by pore-pressure diffusion, or regional tectonic stresses. In the case of dyke propagation, migration can occur at speeds from the order of 0.01 m/s to a few metres per second (Battaglia et al., 2005; Brandsdóttir and Einarsson, 1979; Hayashi and Morita, 2003; Hensch et al., 2008; Klein, 1982; Maccaferri et al., 2016; Passarelli et al., 2018; Peltier et al., 2005; White et al., 2011; Einarsson and Brandsdóttir, 1979; Spence and Turcotte, 1985), while for pore-pressure diffusion or regional tectonic stress triggered migration, speeds of 0.001 m/s up to ~0.3 m/s have been observed (Antonioli et al., 2005; Hensch et al., 2008; Klein et al., 1977; Noir et al., 1997; Passarelli et al., 2018; Shelly et al., 2013; Waite and Smith, 2002).

When migration is slow, larger time windows are needed before trends can be picked up (Fig. 9). To ensure capturing migration for a range of speeds, we therefore used a variety of time window sizes when conducting the trend test for amplitude ratio changes. The selection of which time window sizes to use is flexible.

It is tempting to conclude that when comparing between different migration episodes or different phases in the same migration episode, the relative speed of the seismic migration can be inferred from the minimum time window size required to detect a trend in the amplitude ratio. However, this is only true if the uncertainty of the amplitude ratios is constant, hence the source volume remains unchanged throughout this episode.

5.4. Impact of background noise removal

Fig. 10 demonstrates the importance of background noise removal. If background noise is not removed, the diurnal cycle causes amplitude ratios to change, creating misleading false positives (c.f. Fig. 8). Note the drop in percentage of station pairs showing a change in amplitude ratios

upon losing one station (see discussion Section 5.5) towards the end of the analysis. The selection of both the quiet period and the threshold for background noise removal are important for effective background noise removal. Adjustments could be made to what was described in Section 3.3 as needed, through testing.

5.5. Limitations of the method

1. As seen in the example for Piton de la Fournaise in Section 4.1, detection might be difficult or even impossible if the migration duration is too short. In such cases, if an eruption occurs at the end of the migration, only a very late or no warning could be given.
2. Like with any other seismic location technique, uncertainties will depend on the overall signal-to-noise ratio, as well as the network configuration with respect to the location of the seismic sources. If seismic sources are outside the network and too far away, the differences in relative source-station distances are negligible, so even when there is migration, the amplitude ratios recorded across all stations pairs would essentially stay the same.
3. When the migrating seismicity is only recorded by a small portion of the network, the percentage of station pairs detecting amplitude ratio changes would be low and detection might be missed altogether. This could be overcome by selecting just the stations recording the activity to do the analysis.
4. Strong local wind might generate increase in seismic noise at a few stations that is not removed by the background noise removal process and be misinterpreted as a migration. Although there are possible ways to deal with wind noise, putting too much effort into removing short term changes might remove actual short term seismic migration too.

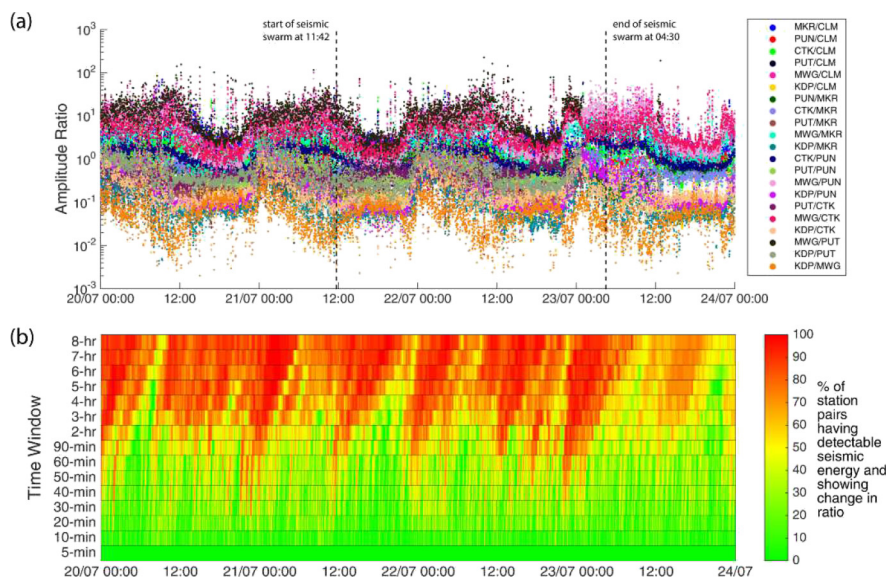


Fig. 10. Results for the seismic swarm at Gede in July 2015, with no removal of background noise. The diurnal cycle is clearly visible. (a). Time series of amplitude ratios for all possible station pairs. (b). Time series showing the percentage of station pairs with detectable seismic energy exhibiting changes in amplitude ratios. Calculation was done with moving windows, shifting by 1 min from one window to the next. Without the removal of background noise, it is impossible to distinguish diurnal cycles from actual migration.

- The proposed approach is tuned for high-frequency, VT type of earthquake associated with pressure/stress changes into the system, as opposed to long-period/hybrid events that are already associated with a fluid phase, and by essence already a concern in terms of changes in the state of the volcano.

We believe our method is robust enough to be applicable for a wide variety of volcanoes. However, it should be used in tandem with other monitoring parameters. The idea of our method is to get a quick yes/no answer on whether there is migration. It would be difficult to judge whether the amplitude changes were caused by a single or multiple sources. It would also be impossible to infer much about the location and direction of migration without either analysing individual amplitude ratios or further analysis like setting up an inverse problem using actual displacement or velocity amplitudes (which would require site amplification factors, instrument response, etc.). While this is possible, it is not our focus and defeats the purpose for a rapid real-time assessment tool.

5.6. Towards practical application

The ultimate aim of this study is to have a practical tool which observatories can use for real-time monitoring of seismic migration. To this end, there are a few points to consider regarding a realistic application and interpretation. Firstly, automated migration detection and alert is essential for a real-time monitoring tool. With Red-flag SARA, it is simple to set a criterion such as: more than X% of seismic station pairs must show a sustained change in amplitude ratios for at least Y hours. When met, a red flag is raised and an alert can be sent to observers. The determination of X and Y would depend on the local conditions (network configuration, typical migration timescales and locations, etc.) and the accepted level of false alarm, with tests done on local datasets. Secondly, it is important to bear in mind that detected migration could either be real or simply an artifact due to a local effect at one particular station in the case of a sparse network. A malfunction or irregularity at one single station will affect all the station pairs in which this station is involved, which could be a significant percentage of station pairs. Taking this into account, the minimal value for X chosen could be the percentage of station pairs affected by one station: $\frac{2}{N} \times 100\%$ (where N is the number of recording stations). Lastly, if the network covers a vast area, migration detection would be more robust if parallel analyses are done – one using all stations and another using a relevant sub-network. The sub-network consisting of stations near to expected migration would enhance detection by discarding station pairs that are less sensitive to or not even recording the migration.

For the datasets for Piton de la Fournaise and Gede that we have tested our tool on, the choice of time windows to use for trend detection as well as the threshold for background noise removal have worked well, although a threshold of 4 median absolute deviations, rather than 3, could be slightly more effective for some cases at Gede (see Appendix E). The selection of the quiet period for background noise removal is important when the background noise levels are not constant. Selecting a period just before the period of interest produces better results as background noise levels would be closer to that during the period of interest. It would however, mean that background noise levels have to be recalculated often when running the tool in real time. An alternative would be to use a very long period for the calculation of the background noise levels.

6. Conclusion

For volcano observatories, extracting as much information as possible about the state of the volcano, and doing it as quickly as possible is crucial, especially during volcanic crises. Our improved SARA method to track magma migration via the time evolution of amplitude ratios

provides an additional potential real-time monitoring parameter to assist observatories in doing so. This method can be employed quickly and without needing any prior knowledge of site and instrument characteristics which traditional amplitude source location methods require. The time evolution and trend is what gives insight, rather than absolute values of seismic amplitude. In addition, the method works for overlapping events recorded as continuous data, and can provide a time series processed in real time just like any other typical monitoring parameter.

We tested our improved SARA method with synthetic as well as real data, and the results are promising. Not only does Red-flag SARA detect the start of seismic migration, but it can also differentiate between seismic episodes ending as an intrusion or a tremor-generating eruption, and, therefore offers indications about the dynamics of the processes driving the migration. We hope that this method would be widely adopted at observatories in future, either in the form of a stand-alone tool, or embedded within existing packages like MSNoise (Lecocq et al., 2014) or WebObs (Beauducel et al., 2010).

Acknowledgements

We gladly thank the Observatoire Volcanologique du Piton de la Fournaise (OVPF) and Centre of Volcanology and Geological Hazards Mitigation (CVGHM) for data collection and for giving us permission to use the data. We would also like to thank Dr. Dannie Hidayat for providing the information regarding the location of the seismic events at Gede.

This work comprises Earth Observatory of Singapore contribution no. 247.

This research is partly supported by the National Research Foundation Singapore and the Singapore Ministry of Education under the Research Centres of Excellence initiative.

Appendix A. Background seismicity

Fig. A.1 and A.2 show the respective results of using distal VTs and seismicity along a local fault as background seismicity before, during and after a vertical migration episode. Distal VTs were simulated by having normally distributed events spread about a point on the flank of the volcano where its distance from the summit is the same as its depth, as commonly found to be (White and McCausland, 2016). As can be seen in Fig. A.1, the amplitude ratios during the migration are still showing the same pattern as before (Fig. 2), except that their level of uncertainty is reduced.

Similar results are obtained for the case of background seismic activity being seismicity along a local fault. Events were normally distributed along a NE-SW trending line at a depth of 10 km (Fig. A.2). Selection of the location of the fault was based on an existing fault at Gede (Nugraha et al., 2017).

Appendix B. Kendall's rank correlation coefficient, τ

Kendall tau coefficient (Kendall and Gibbons, 1990) is defined as the proportion of concordant pairs minus the proportion of discordant pairs:

$$\tau = \frac{(\text{number of concordant pairs}) - (\text{number of discordant pairs})}{\frac{1}{2}(n(n-1))}$$

where n is the number of data points. τ is thus expected to be in the range $-1 \leq \tau \leq 1$, giving a value close to zero when amplitude ratios remain relatively constant, and values closer to ± 1 when amplitude ratios display a trend. If the amplitude ratios undergo a step change, as illustrated in Fig. B.1(a), τ would also produce a value close to ± 1 , even though there is no increasing or decreasing trend. This explains why there is a strong detection at the beginning and ending of the simulated

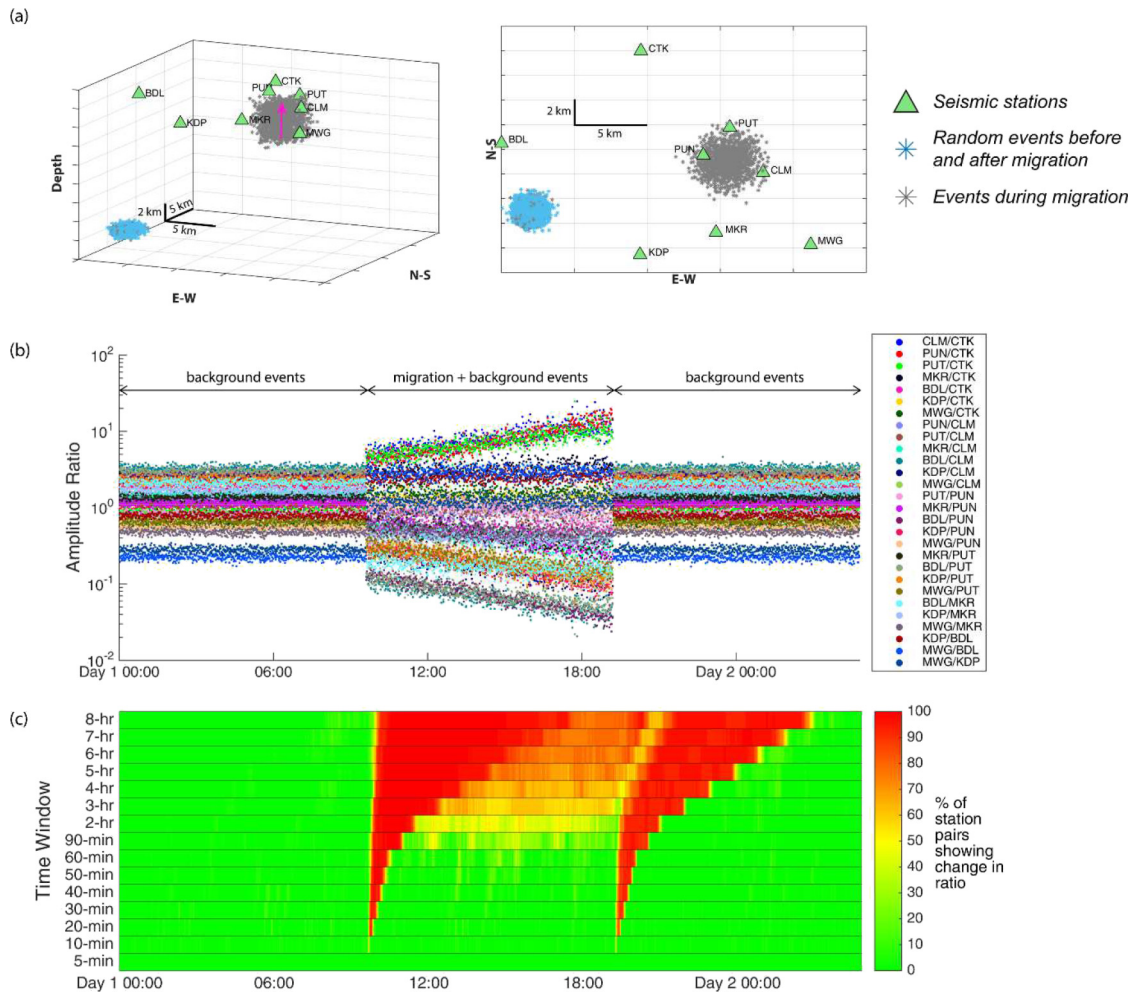


Fig. A.1. Results for simulated vertical migration from 2 km below sea level to 2 km above sea level, with distal VTs as background seismicity. (a). 2-D and 3-D plots showing seismic network and event locations. (b). Time series of amplitude ratios for all possible station pairs. (c). Time series showing the percentage of station pairs exhibiting changes in amplitude ratios. Results are similar to results for random background seismicity spread throughout the network (Fig. 2).

episodes. In the Piton de la Fournaise examples described in Sections 4.1 and 4.2, the strong detection at the beginning and ending of the migration is absent because the background seismicity before and after the migration is weak and hence there are too few data points, like in the extreme case depicted in Fig. B.1 (b).

In Fig. 9, towards the end of the migration, there is a short duration where detection of trend is lost. The amplitude ratio has a decreasing trend, but steps up after the migration ends. Because of this contrast of decreasing and increasing values, at a certain point when the window includes both the decreasing trend and the background seismicity, the number of concordant and discordant pairs become almost equal (Fig. B.2), leading to a non-detection. Later on, when the window includes more of the background and less of the decreasing trend, the number of concordant pairs will dominate and hence lead to detection again.

Appendix C. Migration event rate versus background seismicity event rate

Fig. C.1 shows the effect of relative rates between migration and background seismicity events for the episode of vertical migration described in Fig. 2. The migration speed was set at 10 km/day. At this speed, down to a relative rate of 0.25 between migration and background seismicity events (every 1 migration event is followed

by 4 background events), migration can still be detected when using window sizes of at least 5 h, but at a relative rate of ~0.1, migration is difficult to be detected, and requires window sizes of at least 8 h.

Despite background seismicity event rates being higher than migration event rates, detection of migration is possible because of the way Kendall's correlation coefficient τ (see Appendix B) is calculated – the number of concordant and discordant pairs would not be equal. However, when the background seismicity event rates become much higher than the migration event rates, the number of concordant and discordant pairs would become much closer and τ would approach zero, losing detection.

Appendix D. Amplitude ratio trend reversal

When migration passes relatively near by a station, the ratios involving this station and a station further away can increase then decrease, or vice versa. Fig. D.1 shows three different scenarios where this can occur. To illustrate this effect more clearly, hypothetical stations located at the same elevation were used, and no uncertainty was introduced in the event source locations during the migration. However, source amplitudes were still allowed to randomly vary over two orders of magnitude.

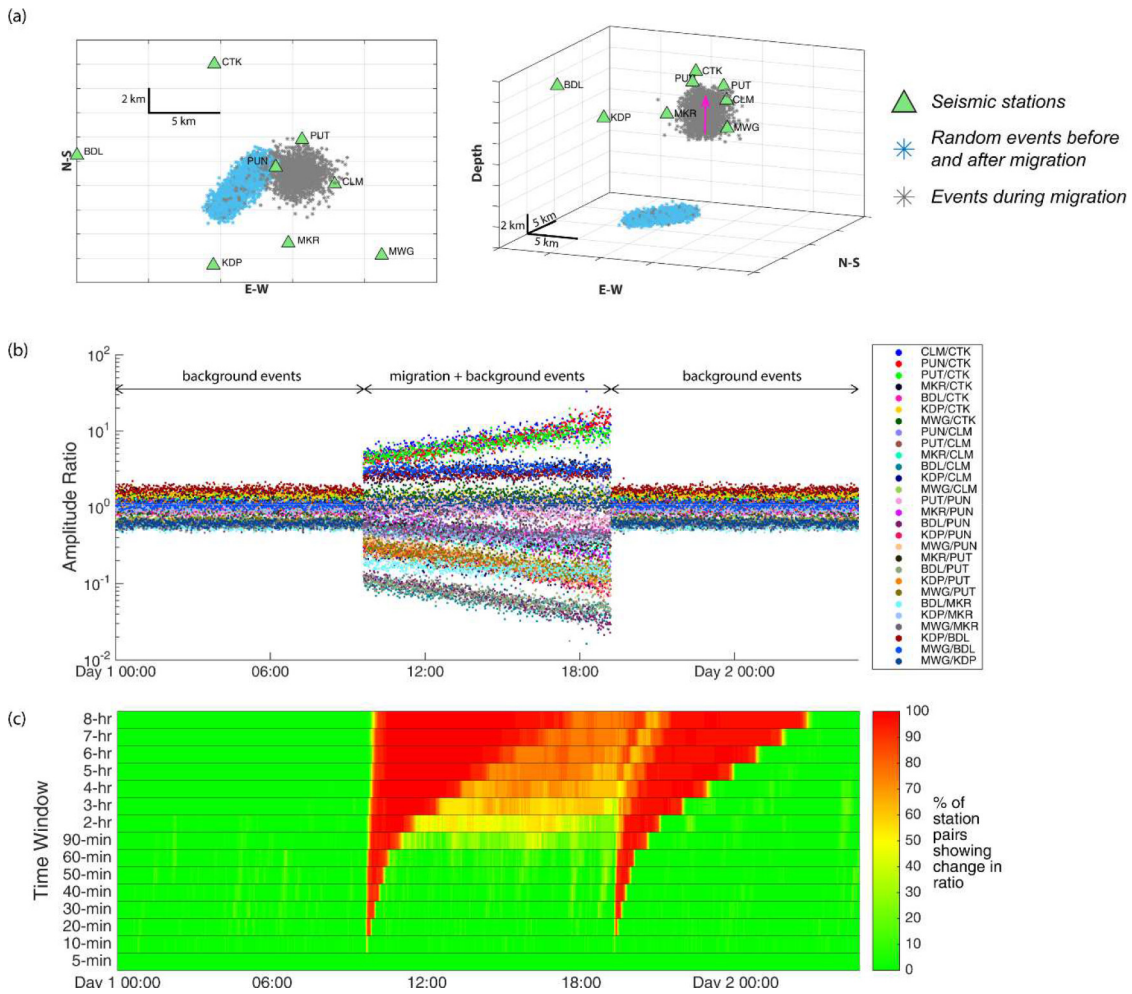


Fig. A.2. Results for simulated vertical migration from 2 km below sea level to 2 km above sea level, with seismicity along a local fault as background seismicity. Panels as for Fig. A.1. Results are again similar to results for random background seismicity spread throughout the network (Fig. 2).

When the window is framing the opposite trends together, the number of concordant and discordant pairs is almost equal and τ approaches zero, resulting in no trend detection (Fig. D.1(d)). However, once the window moves out of the first increasing (or decreasing) part of the time series on to framing only the second decreasing (or increasing) part of the time series, the resultant is a trend detection. This explains the effect seen in Fig. 5(c).

Appendix E. Other Gede swarms

Fig. E.1 and E.2 show two more examples of seismic swarms at Gede where seismicity did not show any obvious migration. For the March 2015 swarm, >110 VT events were recorded over 48 h (PVMBG, 2015b), while for the October 2016 swarm, ~230 VT events were recorded over 4 days (PVMBG, 2016).

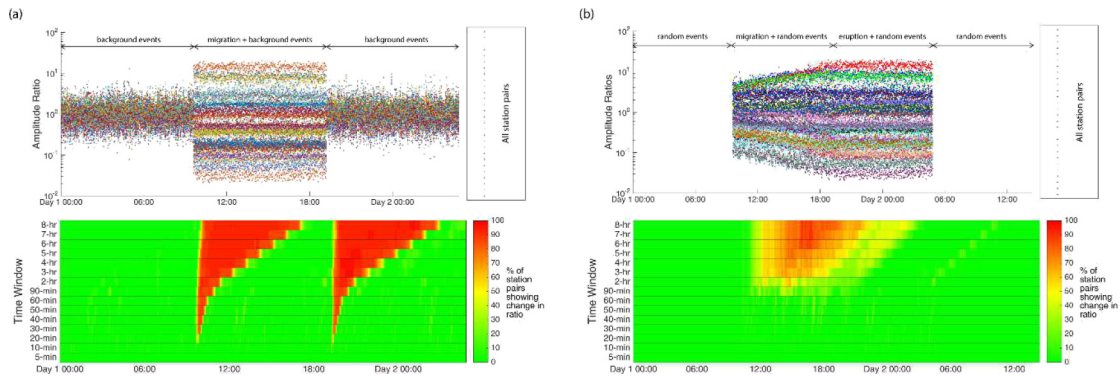


Fig. B.1. (a). Example of the effect a step change in amplitude ratios. The amplitude ratios were simulated by removing the migration section of the vertical migration to eruption example described by Fig. 5. A step change involving all the station pairs results in a strong detection. (b). Example showing how the results for migration and eruption should look like without the influence of a step change before and after the migration and eruption.

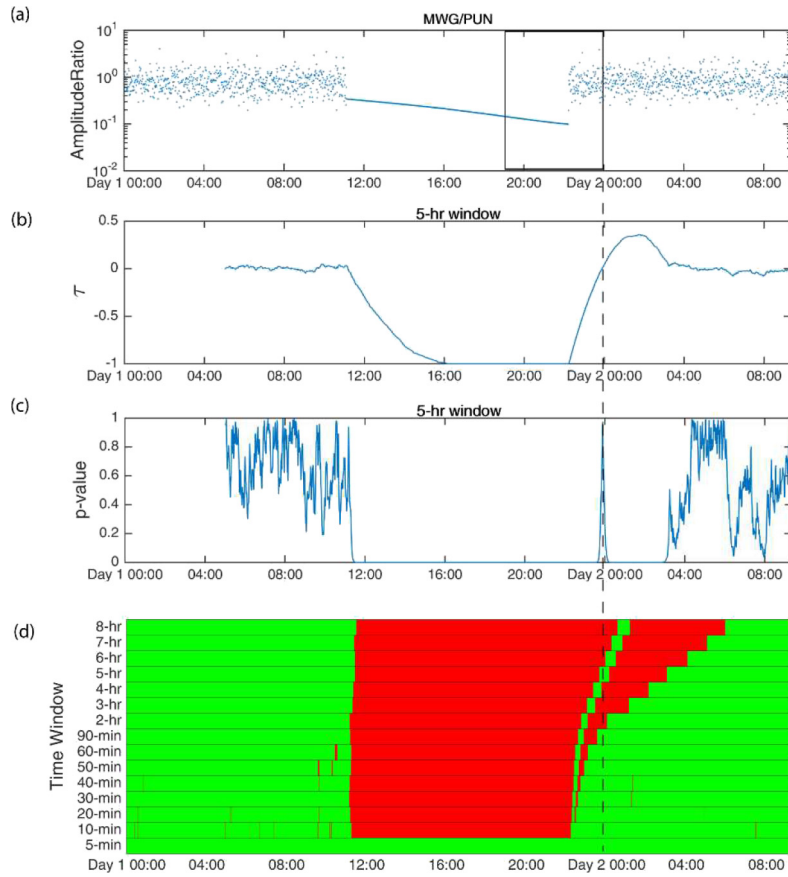


Fig. B.2. Contrasting trend and step at results in loss of trend detection at certain windows. (a). Time series of amplitude ratio for station pair MWG/PUN. (b). Kendall tau coefficient τ calculated over 5-h windows. (c). Corresponding p -values calculated from (b). (d). Time series showing the percentage of station pairs exhibiting changes in amplitude ratios. The window in black has approximately equal proportions of concordant and discordant pairs, resulting in τ being close to 0 and p -value way above the threshold of 0.01, and hence no trend detection.

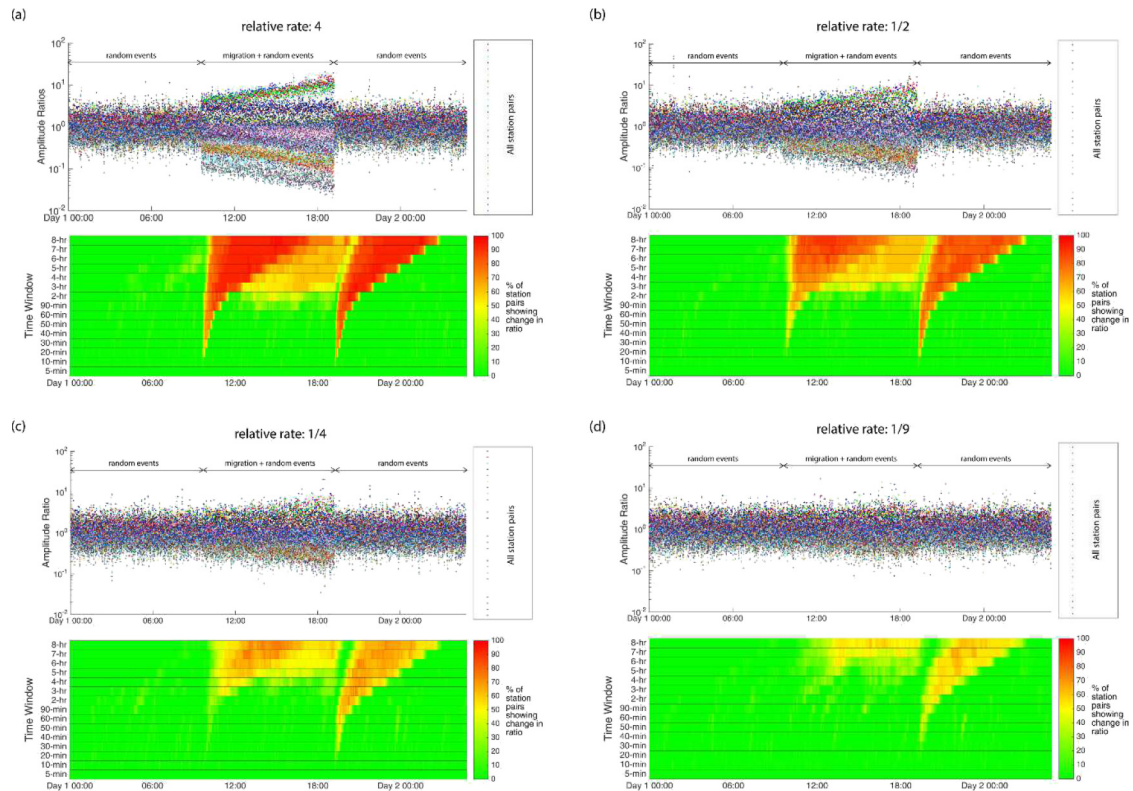


Fig. C.1. Results for simulated vertical migration from 2 km below sea level to 2 km above sea level, with varying relative rates between migration and background seismicity events. Detection is possible even if migration events occur at lower rates than background seismicity events, though at a relative rate of ~ 0.1 (d), detection becomes much more difficult.

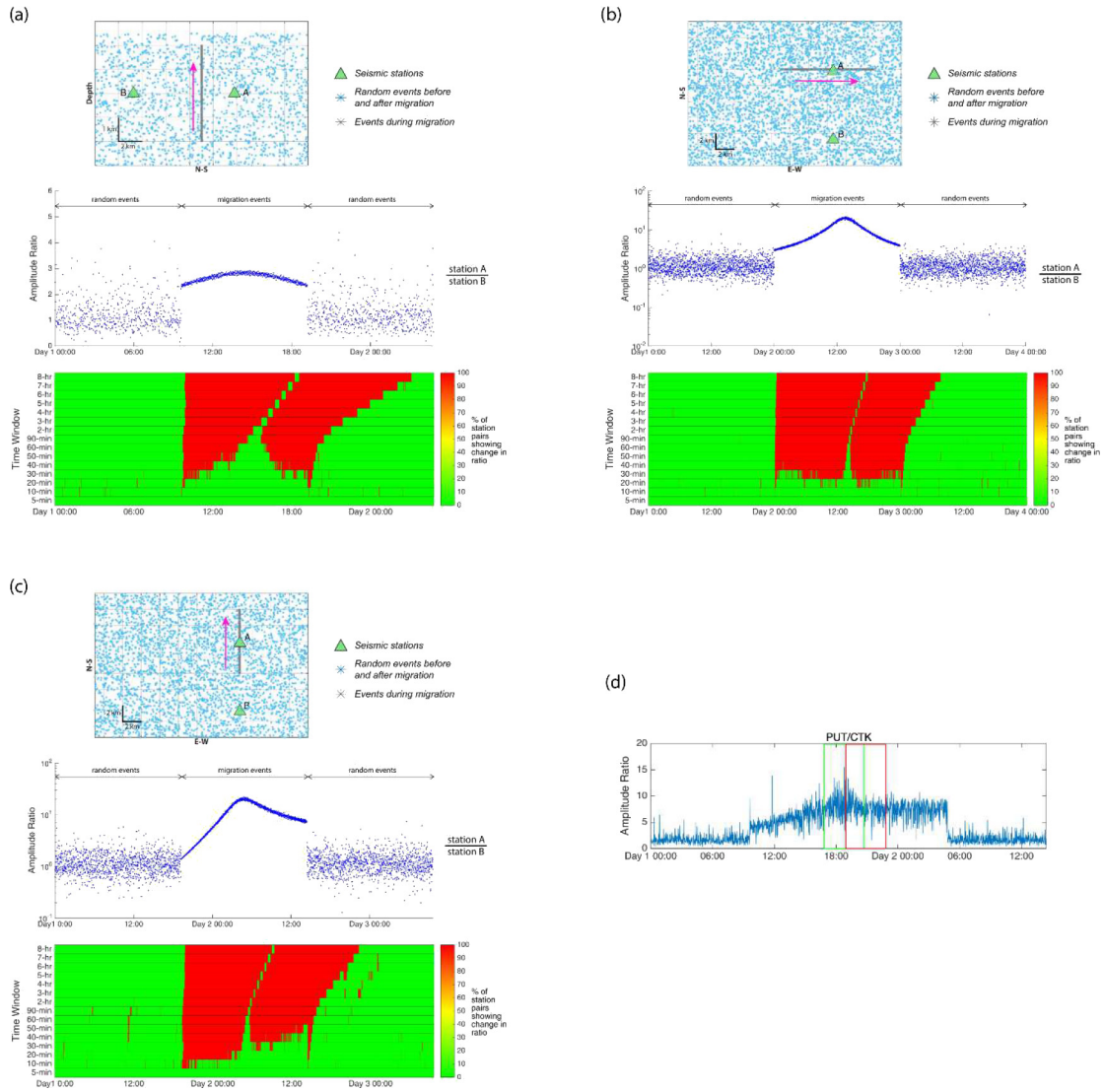


Fig. D.1. (a), (b) and (c). Results for vertical migration, horizontal east-west migration, and horizontal north-south migration respectively. In each case, the amplitude ratio increases then decreases as it passes close by Station A. (d). Amplitude ratio time series for PUT/CTK for the example given in Fig. 5. When the window is framing opposing trends (green rectangle), τ approaches zero, and no trend is detected. When the window frames only the increasing or decreasing part of the time series (red rectangle), trend is detected.

A threshold of 4 median absolute deviations to remove background noise was also tested for these two swarms. Results show a slight improvement in preventing the diurnal cycles from being detected as

migration. The selection of background noise removal threshold should be restrictive enough to eliminate the diurnal cycles but yet not too restrictive such that relevant volcanic seismic energy is also removed.

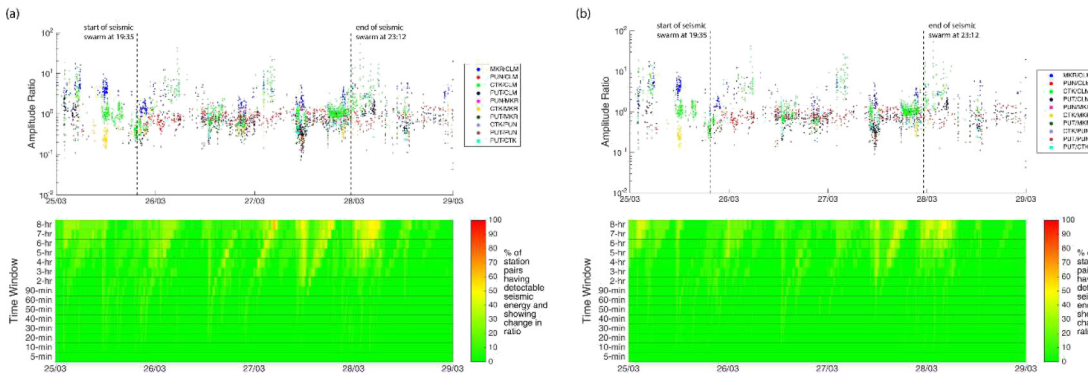


Fig. E.1. Results for seismic swarm at Gede in March 2015. (a). Results using background noise removal threshold of 3 median absolute deviations. (b). Results using background noise removal threshold of 4 median absolute deviations. Slightly more of the effect of diurnal cycles was removed with the use of 4 median absolute deviations.

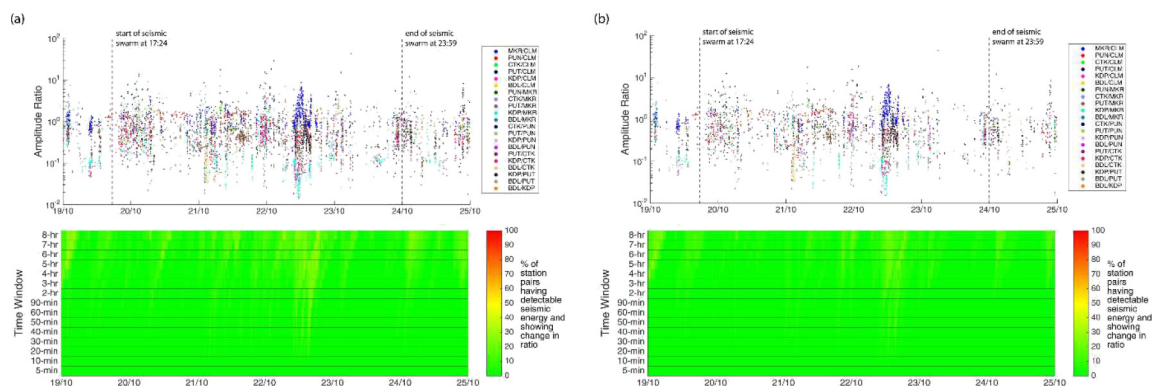


Fig. E.2. Results for seismic swarm at Gede in Oct 2016. (a). Results using background noise removal threshold of 3 median absolute deviations. (b). Results using background noise removal threshold of 4 median absolute deviations. Slightly more of the effect of diurnal cycles was removed with the use of 4 median absolute deviations.

References

- Antonioli, A., Piccinini, D., Chiaraluce, L., Cocco, M., 2005. Fluid flow and seismicity pattern: evidence from the 1997 Umbria-Marche (central Italy) seismic sequence. *Geophys. Res. Lett.* 32, 1–4. <https://doi.org/10.1029/2004GL022256>.
- Battaglia, J., Aki, K., 2003. Location of seismic events and eruptive fissures on the Piton de la Fournaise volcano using seismic amplitudes. *J. Geophys. Res.* 108, 2364. <https://doi.org/10.1029/2002JB002193>.
- Battaglia, J., Ferrazzini, V., Staudacher, T., Aki, K., Cheminée, J.L., 2005. Pre-eruptive migration of earthquakes at the Piton de la Fournaise volcano (Réunion Island). *Geophys. J. Int.* 161, 549–558. <https://doi.org/10.1111/j.1365-246X.2005.02606.x>.
- Beauducel, F., Bosson, A., Randriamora, F., Anténon-Habazac, C., Lemarchand, A., Saurel, J.M., Nercessian, A., Bouin, M.P., de Chabalier, J.B., Clouard, V., 2010. Recent advances in the Lesser Antilles observatories part 2: WebObs-an integrated web-based system for monitoring and networks management. *EGU General Assembly Conference Abstracts* 12, p. 5098.
- Brandssdóttir, B., Einarsson, P., 1979. Seismic activity associated with the September 1977 deflation of the Krafla central volcano in northeastern Iceland. *J. Volcanol. Geotherm. Res.* 6, 197–212. [https://doi.org/10.1016/0377-0273\(79\)90001-5](https://doi.org/10.1016/0377-0273(79)90001-5).
- Caudron, C., Taisne, B., Kugaenko, Y., Saltykov, V., 2015. Magma migration at the onset of the 2012–13 Tolbachik eruption revealed by Seismic Amplitude Ratio Analysis. *J. Volcanol. Geotherm. Res.* 307, 60–67. <https://doi.org/10.1016/j.jvolgeores.2015.09.010>.
- Caudron, C., White, R.S., Green, R.G., Woods, J., Ágústssdóttir, T., Donaldson, C., Greenfield, T., Rivalta, E., Brandssdóttir, B., 2018. Seismic amplitude ratio analysis of the 2014–2015 Bárðarbunga–Holuhraun dike propagation and eruption. *J. Geophys. Res. Solid Earth* 123, 264–276. <https://doi.org/10.1002/2017JB014660>.
- Einarsson, P., Brandssdóttir, B., 1979. Seismological evidence for lateral magma intrusion during the July 1978 deflation of the Krafla Volcano in NE-Iceland. No. UI-79-9-7. University of Iceland, Reykjavik, IS <https://doi.org/10.2172/890964>.
- Hayashi, Y., Morita, Y., 2003. An image of a magma intrusion process inferred from precise hypocentral migrations of the earthquake swarm east of the Izu Peninsula. *Geophys. J. Int.* 153, 159–174. <https://doi.org/10.1046/j.1365-246X.2003.01892.x>.
- Hensch, M., Riedel, C., Reinhardt, J., Dahm, T., 2008. Hypocenter migration of fluid-induced earthquake swarms in the Tjörnes Fracture Zone (North Iceland). *Tectonophysics* 447, 80–94. <https://doi.org/10.1016/j.tecto.2006.07.015>.
- Jolly, A.D., Thompson, G., Norton, G.E., 2002. Locating pyroclastic flows of Soufriere Hills volcano, Montserrat, West Indies, using high dynamic range instruments. *J. Volcanol. Geotherm. Res.* 118, 299–317.
- Kendall, M., Gibbons, J.D., 1990. *Rank Correlation Methods*. 5th edn. Oxford University Press, New York.
- Klein, F.W., 1982. Earthquakes of Loihi submarine volcano and the Hawaiian hot spot. *J. Geophys. Res.* 87, 7719–7726. <https://doi.org/10.1029/JB087iB09p07719>.
- Klein, F.W., Einarsson, P., Wyss, Max, 1977. The Reykjanes Peninsula, Iceland, earthquake swarm of September 1972 and its tectonic significance. *J. Geophys. Res.* 82, 865–888. <https://doi.org/10.1029/JB082i005p00865>.
- Lecocq, T., Caudron, C., Brenguier, F., 2014. MSNoise, a Python package for monitoring seismic velocity changes using ambient seismic noise. *Seismol. Res. Lett.* 85, 715–726. <https://doi.org/10.1785/0220130073>.
- Maccaferri, F., Rivalta, E., Passarelli, L., Aoki, Y., 2016. On the mechanisms governing dike arrest: insight from the 2000 Miyakejima dike injection. *Earth Planet. Sci. Lett.* 434, 64–74. <https://doi.org/10.1016/j.epsl.2015.11.024>.
- Morioka, H., Kumagai, H., Maeda, T., 2017. Theoretical basis of the amplitude source location method for volcano-seismic signals. *J. Geophys. Res. Solid Earth* 122, 6538–6551. <https://doi.org/10.1002/2017JB013997>.
- Noir, J., Jacques, E., Béki, S., Adler, P.M., Tapponnier, P., King, G.C.P., 1997. Fluid flow triggered migration of events in the 1989 Dobi earthquake sequence of Central Afar. *Geophys. Res. Lett.* 24, 2335–2338. <https://doi.org/10.1029/97GL02182>.
- Nugraha, A.K., Maryanto, S., Triastuty, H., 2017. Hypocenter determination and clustering of volcano-tectonic earthquakes in Gede volcano 2015. *J. Neutrino* 9, 44. <https://doi.org/10.18860/neu.v9i2.4103>.
- Observatoire Volcanologique du Piton de la Fournaise (OVPF), 2015. *Observatory Report* (ISSN: 2610-5101-2015/07/31 - 11h30).
- Observatoire Volcanologique du Piton de la Fournaise (OVPF), 2017a. *Observatory Report* (ISSN: 2610-5101-2017/05/21 - 17h00).
- Observatoire Volcanologique du Piton de la Fournaise (OVPF), 2017b. *Observatory Report* (ISSN: 2610-5101-2017/05/23 - 16h30).
- Passarelli, L., Heryandoko, N., Cesca, S., Rivalta, E., Rasmid, A., Rohadi, S., Dahm, T., Milkerreit, C., 2018. Magmatic or not magmatic? The 2015–2016 Seismic Swarm at the Long-Dormant Jailolo Volcano, West Halmahera, Indonesia. *Front. Earth Sci.* 6, 1–17. <https://doi.org/10.3389/feart.2018.00079>.
- Peltier, A., Ferrazzini, V., Staudacher, T., Bachèry, P., 2005. Imaging the dynamics of dyke propagation prior to the 2000–2003 flank eruptions at Piton de la Fournaise, Réunion Island. *Geophys. Res. Lett.* 32, 1–5. <https://doi.org/10.1029/2005GL023720>.
- Pusat Vulkanologi Dan Mitigasi Bencana Geologi (PVMBG) - Bidang Pengamatan Dan Penyelidikan Gunungapi, 2015a. *Laporan Pemantauan Kegiatan Gunungapi Wilayah Barat, Di Indonesia Juli 2015*.
- Pusat Vulkanologi Dan Mitigasi Bencana Geologi (PVMBG) - Bidang Pengamatan Dan Penyelidikan Gunungapi, 2015b. *Laporan Pemantauan Kegiatan Gunungapi Wilayah Barat, Di Indonesia Maret 2015*.
- Pusat Vulkanologi Dan Mitigasi Bencana Geologi (PVMBG) - Tim Kelompok Kerja (Pokja), 2016. *Evaluasi Penerimaan Laporan Dari Pos Pengamatan Gunungapi Oktober 2016*.
- Rubin, A.M., 1993. Tensile fracture of rock at high confining pressure: implications for dike propagation. *J. Geophys. Res.* 98, 15919. <https://doi.org/10.1029/93JB01391>.
- Shelly, D.R., Hill, D.P., Massin, F., Farrell, J., Smith, R.B., Taira, T., 2013. A fluid-driven earthquake swarm on the margin of the Yellowstone caldera. *J. Geophys. Res. E Planets* 118, 4872–4886. <https://doi.org/10.1002/jgrb.50362>.
- Spence, D.A., Turcotte, D.L., 1985. Magma-driven propagation of cracks. *J. Geophys. Res. Solid Earth* 90 (B1), 575–580. <https://doi.org/10.1029/JB090iB01p0575>.
- Taisne, B., Brenguier, F., Shapiro, N.M., Ferrazzini, V., 2011. Imaging the dynamics of magma propagation using radiated seismic intensity. *Geophys. Res. Lett.* 38, 2–6. <https://doi.org/10.1029/2010GL046068>.
- Waite, G.P., Smith, R.B., 2002. Seismic evidence for fluid migration accompanying subsidence of the Yellowstone caldera. *J. Geophys. Res. Solid Earth* 107, 1–15. <https://doi.org/10.1029/2001JB000586> ESE 1-1-ESE.
- White, R., McCausland, W., 2016. Volcano-tectonic earthquakes: a new tool for estimating intrusive volumes and forecasting eruptions. *J. Volcanol. Geotherm. Res.* 309, 139–155. <https://doi.org/10.1016/j.jvolgeores.2015.10.020>.
- White, R.S., Drew, J., Martens, H.R., Key, J., Soosalu, H., Jakobsdóttir, S.S., 2011. Dynamics of dyke intrusion in the mid-crust of Iceland. *Earth Planet. Sci. Lett.* 304, 300–312. <https://doi.org/10.1016/j.epsl.2011.02.038>.